ISSN 1063-780X, Plasma Physics Reports, 2017, Vol. 43, No. 7, pp. 711–719. © Pleiades Publishing, Ltd., 2017.
Original Russian Text © S.I. Lashkul, A.B. Altukhov, A.D. Gurchenko, E.Z. Gusakov, V.V. Dyachenko, L.A. Esipov, M.A. Irzak, M.Yu. Kantor, D.V. Kouprienko, A.A. Perevalov, A.N. Saveliev, A.Yu. Stepanov, S.V. Shatalin, 2017, published in Fizika Plazmy, 2017, Vol. 43, No. 7, pp. 593–601.

TOKAMAKS

Transition into the Improved Core Confinement Mode as a Possible Mechanism for Additional Electron Heating Observed in the Lower Hybrid Current Drive Experiments at the FT-2 Tokamak

S. I. Lashkul[a], *, A. B. Altukhov[a], A. D. Gurchenko[a], E. Z. Gusakov[a], V. V. Dyachenko[a], L. A. Esipov[a], M. A. Irzak[a], M. Yu. Kantor[a], D. V. Kouprienko[a], A. A. Perevalov[b], A. N. Saveliev[a], A. Yu. Stepanov[a], and S. V. Shatalin[b]

[a] *Ioffe Institute, St. Petersburg, 194021 Russia*
[b] *St. Petersburg Politechnical University, St. Petersburg, 195251 Russia*
**e-mail: Serguey.Lashkul@mail.ioffe.ru*

Received July 21, 2016; in final form, January 16, 2017

Abstract—In experiments on lower hybrid current drive (LHCD) carried out at the FT-2 tokamak, a substantial increase in the central electron temperature $T_e(r = 0$ cm) from 550 to 700 eV was observed. A complex simulation procedure is used to explain a fairly high LHCD efficiency and the observed additional heating, which can be attributed to a transition into the improved core confinement (ICC) mode. For numerical simulations, data obtained in experiments with deuterium plasma at $\langle n_e \rangle = 1.6 \times 10^{19}$ m^{-3} were used. Simulations by the GRILL3D, FRTC, and ASTRA codes have shown that the increase in the density and central temperature is apparently caused by a significant suppression of heat transport in the electron component. The mechanism for transition into the improved confinement mode at $r < 3$ cm can be associated with the broadening of the plasma current channel due to the lower hybrid drive of the current carried by superthermal and runaway electrons. In this case, the magnetic shear $s = (r/q)(dq/dr)$ in the axial region of the plasma column almost vanishes during the RF pulse. In this study, the effect of lower hybrid waves on the plasma parameters, resulting in a transition into the ICC mode, is considered. New experimental and calculated data are presented that evidence in favor of such a transition. Special attention is paid to the existence of a threshold for the transition into the ICC mode in deuterium plasma.

DOI: 10.1134/S1063780X1707008X

1. INTRODUCTION

The development of methods for noninductive drive of a quasi-stationary plasma current in a tokamak is one of the most challenging problems on the way to creating a fusion reactor [1]. Lower hybrid current drive (LHCD) is an efficient method for sustaining the plasma current and modifying the plasma current profile in order to decrease the magnetic shear $s = (r/q)(dq/dr)$ in the energy deposition region. This enables one to locally reduce the electron heat transport. The mechanism for transport suppression is associated with the formation of a configuration with a negative magnetic shear [2, 3]. In this work, we present results of experimental studies of these effects. The experiments were carried out at the FT-2 tokamak with a major radius of $R_0 = 0.55$ m and minor radius of $a = 0.08$ m, which is specified by a poloidal diaphragm [4]. The main parameters of the facility are as follows: the toroidal magnetic field is $B_T \leq 3$ T, the plasma current is $I_{pl} = 19$–40 kA, the discharge duration is $\Delta t_{pl} =$ 50 ms, the duration of the pumping RF pulse is $\Delta t_{RF} =$ 5–10 ms, the pumping wave frequency is $f_0 =$ 920 MHz, and the input RF power is $P_{RF} < 200$ kW.

The interaction between lower hybrid waves and plasma in the FT-2 tokamak have been carried out for a long time. In particular, the LHCD efficiency was studied [4, 5]. The goal of this work is to analyze the effect of additional electron heating in the plasma core and correlate this effect with the change in the safety factor profile $q(r) = (r/R)B_T/B_\theta$, where B_θ is the poloidal magnetic field.

The experimental conditions and methods of data processing are described in Section 2. In Section 3, the experimental data are compared with the results obtained at larger tokamaks. The efficient central electron heating observed during LHCD is analyzed in Section 4. The simulation results allowing one to explain the mechanism of central plasma heating are discussed in Section 5. The final section summarizes

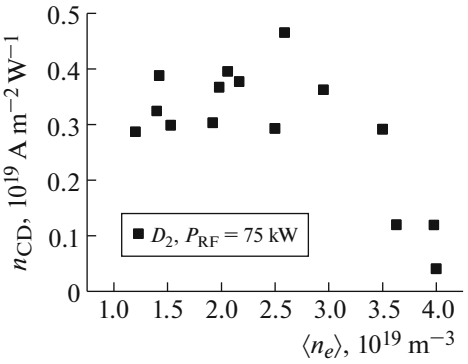

Fig. 1. LHCD efficiency $\eta_{CD} = I_{RF}^N \langle n_e \rangle$ for deuterium plasma.

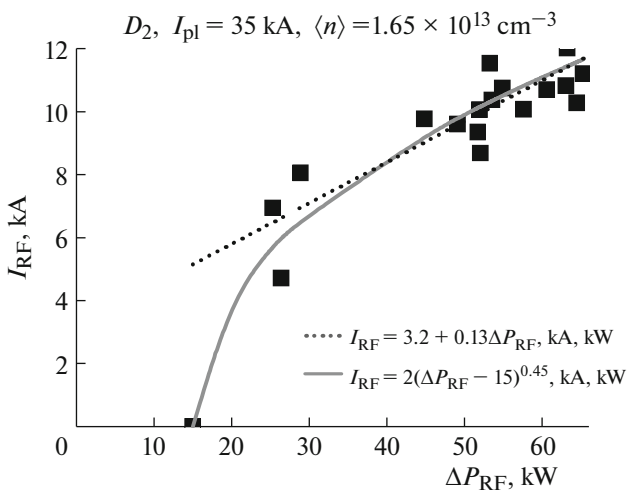

Fig. 2. Current I_{RF} vs. absorbed RF power $\Delta P_{RF} = P_{RF\,inp} - P_{RF\,refl}$ in experiments carried out at $I_{pl} = 35$ kA and $\langle n_e \rangle = 1.6 \times 10^{19}$ m^{-3}.

the results of numerical simulations and processing of the experimental data.

2. DIAGNOSTIC TECHNIQUES AND EXPERIMENTAL RESULTS

In the quasi-stationary stage of the discharge, the RF power at a frequency of $f = 920$ MHz was introduced in the plasma with the help of a two-waveguide grill installed on the low-field side of the torus. The power supply system of the tokamak provided stabilization of the plasma current under LHCD conditions, which resulted in a decrease in the loop voltage ΔU_{pl} proportional to the driven current I_{RF}. The plasma parameters were monitored by means of multipass Thomson scattering (TS) diagnostics, a neutral charge-exchange particle analyzer (NPA), a 2-mm interferometer, hard X-ray (HXR) and soft X-ray (SXR) diagnostics, optical spectroscopy, bolometric measurements, and other diagnostics. The parameters of superthermal and runaway electrons generated during LHCD and contributing to the I_{RF} current were determined using an X-ray spectrometer [6], which detected HXR photons with energies of $E_{h\nu} > 0.2$ MeV. Analysis of the HXR bremsstrahlung spectrum has shown that energies of the generated superthermal and runaway electrons falling onto the chamber wall and diaphragm are in the range from 0.5 to 2.5 MeV and reach $E_{h\nu} \sim 4$ MeV as the loop voltage increases in the post-heating stage of the discharge [6].

3. COMPARISON OF THE LHCD EFFICIENCY WITH THE DATA OBTAINED AT LARGER FACILITIES

In spite of the small dimensions and moderate plasma parameters of the FT-2 tokamak and [4, 5], the value and functional dependence of the LHCD efficiency $\eta_{CD} = I_{RF}^N \langle n_e \rangle$, where $I_{RF}^N = I_{RF} R_0 / P_{RF}$ is the normalized driven current and $\langle n_e \rangle$ is mean plasma density, are close to those typical of large tokamaks [7, 8]. The current I_{RF} was determined from the relation $I_{RF} = \Delta U_{pl} I_{OH} / U_{OH}$, where I_{OH} and U_{OH} are the ohmic current and voltage, respectively. The results of measurements of the LHCD efficiency in deuterium plasma at a current of $I_{pl} = I_{RF} + I_{OH} = 35$ kA, an average electron temperature of $\langle T_e \rangle = 390$ eV, and an effective charge $Z_{eff} \approx 2$ are shown in Fig. 1. It can be seen that, in the range of $\langle n_e \rangle = 10^{19}$ m^{-3}–3×10^{19} m^{-3}, the efficiency η_{CD} is about 0.4×10^{19}A m^{-2} W^{-1}, which corresponds to the data obtained at the FTU, TS, JT-60, ASDEX, and JET tokamaks (Fig. 6 in [7]).

The experimental dependences of the current I_{RF}^N on the main plasma parameters I_{pl}, T_e, and P_{RF} also correspond to those obtained at large facilities [8]. For example, for deuterium plasma, the observed dependence of the current I_{RF} on the absorbed RF power (the difference between the incident and reflected powers) $\Delta P_{RF} = P_{RF\,inp} - P_{RF\,refl}$ at a current of $I_{pl} = 35$ kA and density of $\langle n_e \rangle = 1.6 \times 10^{19}$ m^{-3} (Fig. 2) is close to the results obtained at the Tore Supra, JET, JT-60, and ASDEX tokamaks, where $I_{RF} \sim P_{RF}^{0.65}$. The data presented in Fig. 2 can be approximated to within measurement errors by either a linear dependence or a power law $I_{RF} \sim \Delta P_{RF}^{\alpha}$, where $\alpha = 0.5 \pm 0.1$.

4. EFFECT OF CENTRAL ELECTRON HEATING IN DEUTERIUM PLASMA

Figures 3 and 4 show variations in the main plasma parameters during the interaction between lower hybrid waves and deuterium plasma at a density of

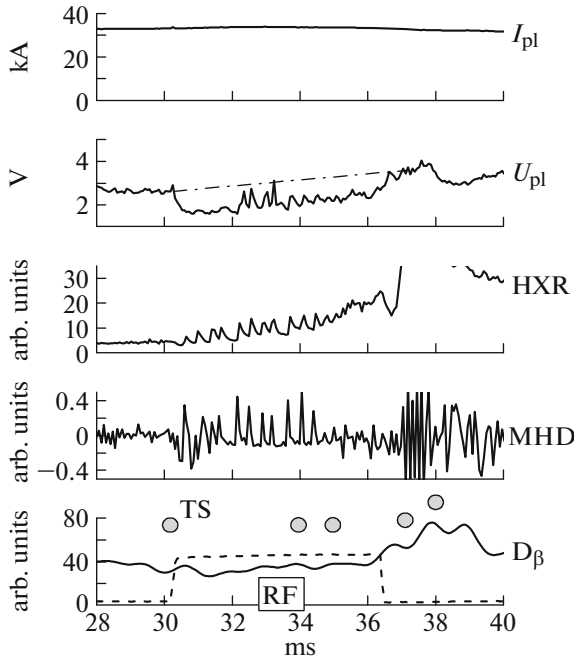

Fig. 3. Waveforms of the I_{pl}, U_{pl}, HXR, MHD, D_β, and P_{RF} signals recorded in an LHCD experiment with $\Delta P_{RF} \approx 63$ kW. The gray circles show the times at which the profiles $T_e(r)$ were measured by the TS diagnostics. The dash-dotted line in the plot of the loop voltage shows the time dependence of the voltage U_{pl} calculated by the ASTRA code for the OH mode in which the effective charge Z_{eff} increases from 1.5 to 2.5.

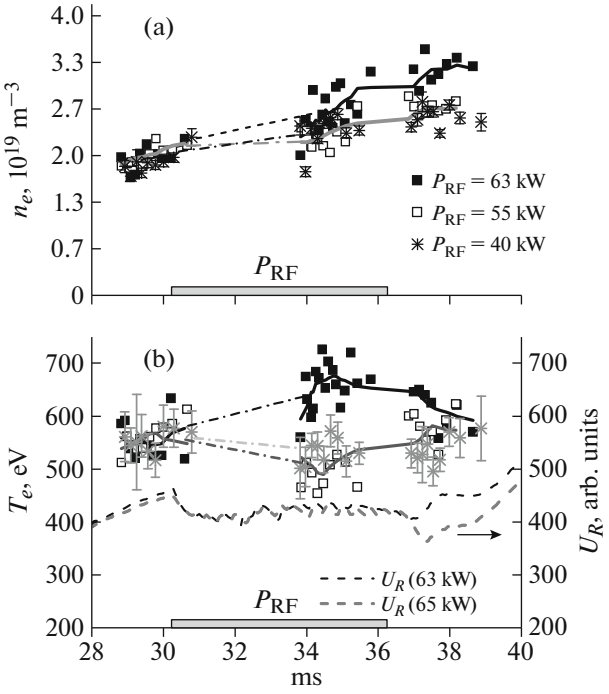

Fig. 4. Time evolution of the (a) central density n_e(x = 1.5 cm, y = 0 cm) and (b) central electron temperature T_e (x = 1.5 cm, y = 0 cm) measured by the TS diagnostics for different input powers ΔP_{RF}. Here, U_R is the signal from the balance detector along the major radius R.

$\langle n_e \rangle = (1.6–1.9) \times 10^{19}$ m^{-3} (the density at which parametric effects and generation of fast ions are insignificant and the efficiency η_{CD} is maximal [5]). Figure 3 shows the time dependences of I_{pl}, U_{pl}, HXR, MHD, D_β, and P_{RF} obtained in the LHCD experiment ($\Delta P_{RF} \approx 63$ kW). The gray circles indicate the times at which the profiles $T_e(r)$ were measured by the TS diagnostics. For comparison with the ohmic heating (OH) mode, the dash-dotted line in the plot of the loop voltage shows the time dependence of the voltage U_{pl} calculated by the ASTRA code for the OH mode in which the effective charge Z_{eff} increases from 1.5 to 2.5, which corresponds to the change in the effective charge Z_{eff} during the RF pulse. The change in the effective charge Z_{eff} from 1.5 to 2.5 associated with the additional heating during the RF pulse will be discussed below (see also Section 5). The measurements show that, at substantially low input powers, $\Delta P_{RF} = P_{input} - P_{output} < 60$ kW, the electron component is cooled in the entire plasma volume. The central electron temperature $T_e(y = 0$ cm) measured by the TS diagnostics decreases from 550 to 500 eV (see Fig. 4b). Electron cooling occurs against the background of a continuous increase in the density, which is confirmed by the data presented in Fig. 4a for the central region of the discharge. However, when the input power reaches a certain threshold value of $\Delta P_{RF}^{th} \geq 63$ kW, a considerable increase in the central electron temperature is observed. During the RF pulse, the temperature increases from 550 to 700 eV. Typically, as the duration of the RF pulse increases, such high values of the central electron temperature are preserved almost up to the end of the RF pulse (Fig. 5). In all cases, termination of the RF pulse is accompanied by the onset of the $m = 2$, $n = 1$ mode and an HXR burst typical of similar experiments carried out at other facilities [2]. The profiles of the main plasma parameters shown in Figs. 6 and 7 for $\Delta P_{RF}^{th} \geq 63$ kW were obtained in a series of similar discharges of the facility. It is seen that, as the discharge periphery cools, the central electron temperature increases considerably. At the same time, a continuous growth and broadening of the density profile is observed during LHCD. It is worth noting that the observed growth of the density cannot be explained by an increase in the intensity of recycling of the working gas at the periphery, because the intensity of the D_β line measured along the central chord (Fig. 3, the bottom plot) remains almost unchanged. Comparison of the intensity of the D_β line with the influx of the neutral gas from the chamber wall [9] allows us to assume that, during the RF pulse, the recycling of the working gas at the periphery of the dis-

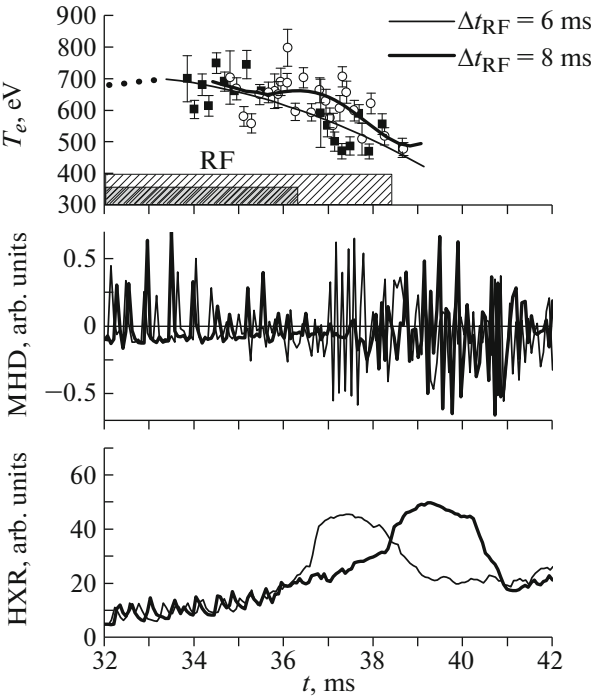

Fig. 5. Effect of the maintenance of the high central temperature as the RF pulse duration increased from 6 to 8 ms. Simultaneously, there is a time shift in the beginning of the growth of MHD oscillations ($m = 2$, $n = 1$) and HXR signals after the end of the RF pulse.

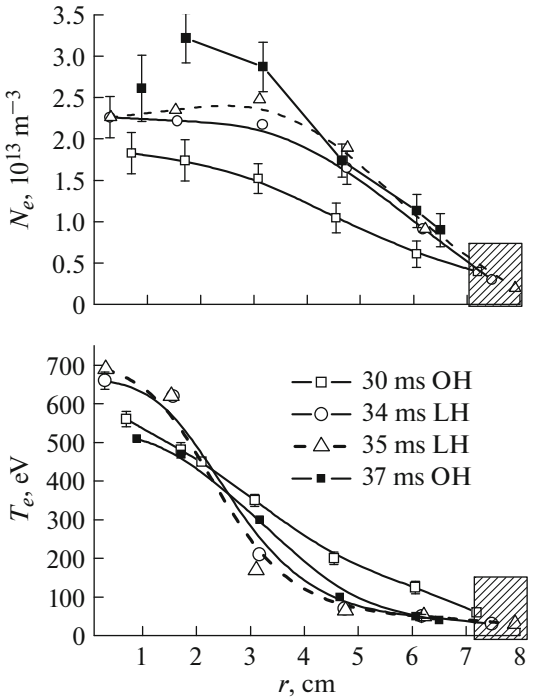

Fig. 6. Time evolution of the plasma density profile $n_e(r)$ and temperature profile $T_e(r)$ measured by the TS diagnostics.

charge remains unchanged or even decreases. This conclusion is confirmed by the chord profiles of the D_β line intensity obtained by rapid scanning in the vertical plane of the tokamak cross section (the scanning time is 1.3 ms). Such measurements were carried out in the similar LHCD shot no. 051216_30. The results of these measurements are presented in Fig. 8. Here, the narrowing of the chord profile due to a considerable decrease in the radiation intensity at the periphery of the discharge was observed (Fig. 8b). In this case, the average density $\langle n_e \rangle$ measured by the interferometer along the central chord grew monotonically, while the intensity of the D_β line along the central chord of the chamber remained almost unchanged (Fig. 8a). The constancy of radiative losses from the discharge periphery indicates that the increase in the density also cannot be related to the additional influx of impurities (Fig. 7). At the same time, the observed increase in the radiation intensity $P_{rad} = \Delta E \langle n_e \rangle \langle n_i \rangle$ from the plasma core during LHCD can be explained by both the growth of the plasma density and the increase in the concentration of ions in high ionization states. At a temperature of T_e = 550–700 eV, most of multiply charged ions are hydrogen-like ions of light impurities, O^{7+} and C^{5+}. The increase in density of highly ionized impurities can be explained by both additional ionization of the impurities already present in the discharge and improved confinement of charged particles in the plasma core. Thus, the experiments indicate that the increase in the plasma density during LHCD is caused by additional ionization and improved confinement of charged particles (which occurs due to a decrease in the diffusion coefficient $D_{e\,\mathrm{eff}}$ [9, 10]), rather than by the increase in the intensity of recycling of the working gas and the additional influx of impurities into the edge plasma. This conclusion is confirmed by new experimental data obtained with the help of the HELIOS diagnostics (additional pulsed puffing of He into deuterium plasma) [11]. The transition into ICC mode (i.e., a decrease in heat transport

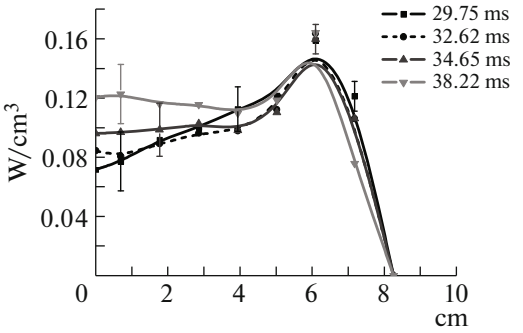

Fig. 7. Time evolution of the radiative loss profile $P_{rad}(r)$ measured by a scanning pyroelectric bolometer.

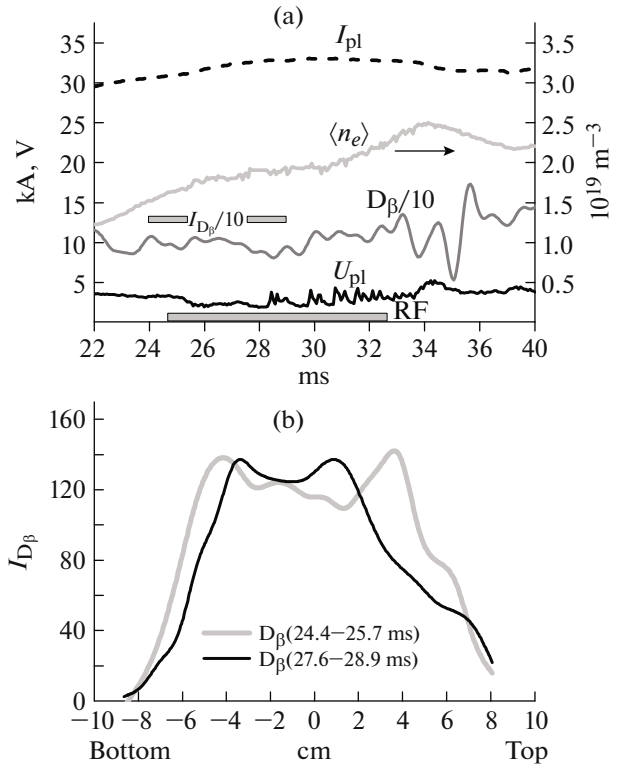

Fig. 8. (a) Waveforms of the I_{pl}, U_{pl}, D_β, and $\langle n_e \rangle$ signals recorded in LHCD shot no. 051216_30 with an input power of $\Delta P_{RF} \approx 106$ kW; (b) chord profiles of the D_β signal. The gray rectangles in panel (a) show the time intervals in which the D_β line emission was measured.

in the plasma core) can also explain the observed spontaneous growth of the central electron temperature $T_e(0)$ after the threshold power level of $\Delta P_{RF} \approx 63$ kW is reached. Indeed, it is hardly possible that electrons in the plasma core are heated due to energy exchange with superthermal and runaway electrons additionally generated by the relatively short RF pulse, because the time required for collisional thermalization of fast electrons with energies of $E = 0.2$–1 MeV is about $t_E \approx 100$–200 ms, which is much longer than the duration of the RF pulse, $\Delta t_{RF} = 6$ ms.

5. NUMERICAL SIMULATIONS AND DISCUSSION OF THE EFFECT OF CENTRAL PLASMA HEATING DURING LHCD

To interpret the experimental results indicating the high LHCD efficiency ($\eta_{CD} \approx 0.4 \times 10^{19}$ A m^{-2} W^{-1}) and test the hypothesis on the transition into the regime of improved particle and energy confinement, we performed complex simulations of the propagation and absorption of lower hybrid waves in the FT-2 plasma. We used the GRILL3D, ASTRA, and FRTC software packages and employed the measured values of plasma parameters obtained at a current of $I_{pl} = 32$ kA.

The GRILL3D code [12] was used to calculate the $P(N_z)$ spectrum of the longitudinal refractive index $N_\parallel = N_z$ (the longitudinal slowing-down factor) of a lower hybrid wave launched into the plasma by a two-waveguide antenna. This spectrum $P(N_z)$ is bidirectional with respect to the plasma current and has several maxima. For example, at a phase shift between the waveguides of $\Delta\varphi = \pi/2$, there are maxima at $N_z \approx -9$, -1.7, 3, and 20 [4].

The magnitude and direction of the current generated by the lower hybrid wave were calculated using the Fast Ray Tracing Code (FRTC) [13], the calculated $P(N_z)$ spectrum, and the measured values of the plasma parameters. In this case, the magnetic equilibrium of the plasma column was calculated by the ASTRA code with the use of the measured radial profiles of the plasma parameters.

We note that these calculations were not self-consistent, because they did not take into account time variations in the plasma parameters. Moreover, the simulations performed with the current version of the FRTC did not take into account the effect of the residual toroidal electric field on the generation of superthermal electron beams. Nevertheless, these simulations allowed us to reveal the governing role of the synergetic effect associated with the effect of the different components of the spectrum of the lower hybrid wave on the plasma processes [4]. It was found that, for plasma with a central temperature of $T_e(0) \sim 0.5$ keV, efficient LHCD by waves with the slowing-down factor of $N_\parallel = -1.8$ is possible only if the spectrum also includes waves with $N_\parallel = -9$, which, themselves, also cannot provide an appreciable current drive. In the given approximation, we obtained data on the radial profiles of the density of the lower hybrid driven current J_{RF} for two densities of deuterium plasma: $\langle n_e \rangle = 1.2 \times 10^{19}$ and 1.9×10^{19} m^{-3} (see Fig. 9). All the plasma parameters used in the simulations corresponded to the experimental data obtained at a current of $I_{pl} = 32$ kA.

To estimate the profile of the total plasma current density ($I_{OH} + I_{RF}$), we assumed that the profile of the current I_{RF}, which is carried by the superthermal electrons in the presence of the residual vortex toroidal electric field, corresponded to the profile shown in Fig. 9a. For the known time evolution of the effective charge Z_{eff}, the currents I_{RF}, I_{OH}, and ($I_{OH} + I_{RF}$) can be calculated by the ASTRA code with the use of the experimental data. Figure 10 shows the time dependence of the effective charge Z_{eff} averaged over the cross section of the plasma column during the RF pulse, obtained by linear interpolation between the its values before and after the RF pulse ($t = 29$ and 38 ms). We also compared the measured and calculated values of the loop voltage, U_{exp} and U_{simul}. The

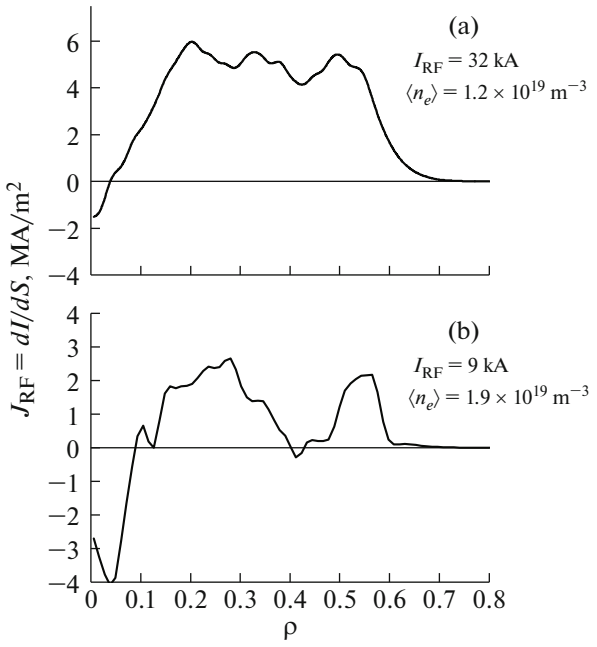

Fig. 9. Radial profiles of the LHCD density $J_{RF}(\rho)$ in deuterium plasma, calculated by the FRTC for $I_{pl} = 30$ kA and two values of the average plasma density: $\langle n_e \rangle$ = (a) 1.2×10^{19} m^{-3} and (b) 1.9×10^{19} m^{-3}. For each value of $\langle n_e \rangle$, the calculated values of the integral current I_{RF} are given.

absolute value of the effective charge Z_{eff} was chosen such that U_{exp} and U_{simul} coincided at any time during ohmic heating. Thus, for shot no. 141504_08, the increase in the average effective charge Z_{eff} from 1.5 to 2.2 after the input of the lower hybrid waves indicates a decrease in the plasma electric conductivity of $\sigma \propto \int_r T_e^{3/2}/Z_{eff} r dr$, which can be due to the cooling of the plasma periphery and the accumulation of impurities in high ionization states (O^{8+} and C^{6+}). In this case, the recycling of the working gas and impurities at the periphery remains the same or even decreases, which is confirmed by measurements of the intensity of the D_β spectral line (Figs. 3, 8) and the dynamics of the radiative loss profiles (Fig. 7). The total current $I_{pl} = I_{RF} + I_{OH}$ shown in Fig. 11 is the sum of the RF current I_{RF} carried by accelerated electrons and the residual ohmic current I_{OH}. Thus, in the first approximation, the shape of the $J_{RF}(r)$ profile was chosen in accordance with Fig. 9a and the absolute values of the current density $J_{RF}(r)$ were obtained by interpolation of the loop voltage U_{simul} with the help of the ASTRA code by adjusting the current I_{RF}. As a result of such an adjustment of the I_{RF} current and, therefore, the calculated values $J_{RF}(r)$, the loop voltage U_{simul} corresponded to the measured values of U_{exp} at any time during and after the RF pulse (see Fig. 10). The simulation results show that the profile of the total current density $J_{sum}(r, t = 34\text{ ms}) = J_{RF}(r, t = 34\text{ ms}) + J_{OH}(r, t = 34\text{ ms})$ in the current drive regime should be broader than the initial profile $J_{OH}(r, t = 30\text{ ms})$ (see Fig. 12). Such a broadening of the current profile in the center of the plasma column should result in the flattening of the safety factor profile $q(r)$ in this region. As a result, the magnetic shear $s = (r/q)(dq/dr)$ in the central region can vanish or even become negative (Fig. 12). Similar experiments carried out at the Tore Supra and JET tokamaks [2, 3] showed that, under these conditions, heat transport should be suppressed. This conclusion was obtained using a transport code describing electron heat transport in the Bohm or gyro-Bohm model [2]. The suppression of heat transport in the entire region with the low magnetic shear was attributed to the decoupling of toroidally coupled modes, which, in turn, resulted in a decrease in the

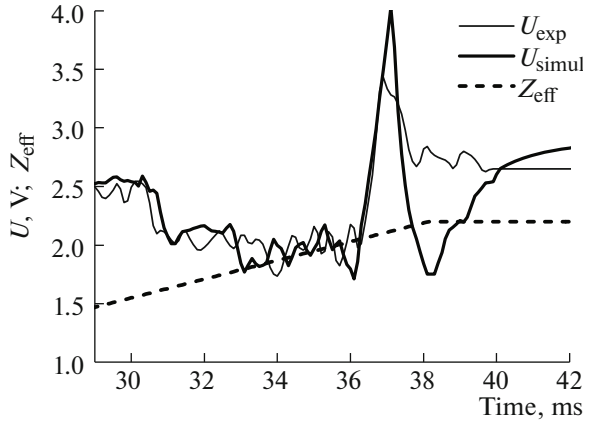

Fig. 10. Comparison of the measured, $U_{exp}(t)$, and calculated, $U_{simul}(t)$, values of the loop voltage in shot no. 041514_08. The calculated time dependence of the effective charge Z_{eff} during the RF pulse is also shown.

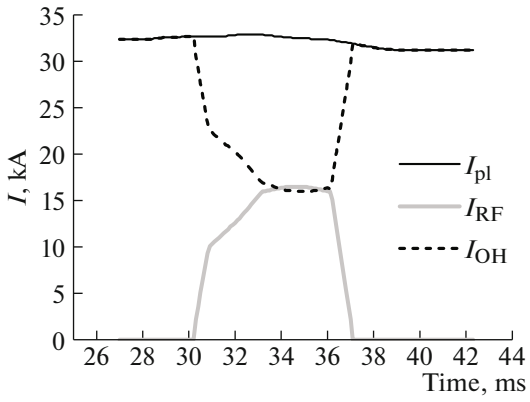

Fig. 11. Time evolution of the RF current I_{RF} and residual OH current I_{OH} determined with allowance for the constancy of the total plasma current I_{pl} ($I_{pl} = I_{RF} + I_{OH}$).

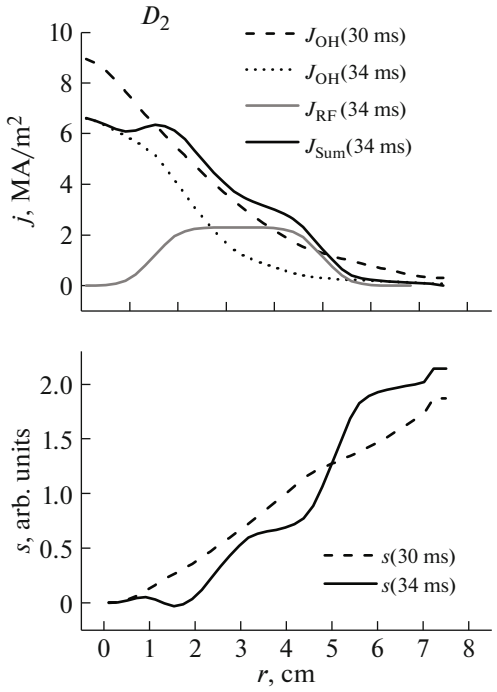

Fig. 12. Calculated profiles of the current densities and the magnetic shear s in the OH stage (30 ms) and during the RF pulse (34 ms). Here, $J_{sum}(r, t = 34\ \text{ms}) = J_{RF}(r, t = 34\ \text{ms}) + J_{OH}(r, t = 34\ \text{ms})$.

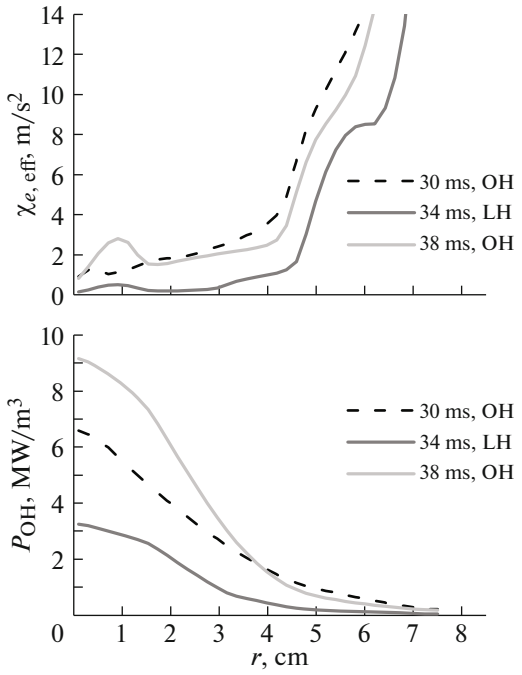

Fig. 13. Profiles of the OH power P_{OH} and effective electron thermal diffusivity $\chi_{e\,eff}$.

radial correlation length of plasma fluctuations [14]. In accordance with this model, it can be assumed that, in spite of a decrease in the residual OH power P_{OH} ($t = 34$ ms) (see Fig. 13), suppression of heat transport caused by a decrease in the magnetic shear to $s \le 0$ leads to an increase in the temperature T_e at $r < 3$ cm. The electron thermal diffusivity $\chi_{e\,eff}$ ($t = 34$ ms) calculated by the ASTRA code is substantially lower than its initial value determined for $t = 30$ ms in the ohmic stage of the discharge (see Fig. 13).

Of course, the above simulations are approximate, because they are based on data on the radial profiles of the driven current density J_{RF} calculated using the non-self-consistent version of the FRTC code without allowance for the effect of the vortex electric field. Nevertheless, they evidence in favor of the hypothesize that the plasma current profile should broaden in the course of LHCD. Unfortunately, no direct measurements of the profile of the plasma current density were carried out. Therefore, to verify the hypothesis on the broadening of the plasma current channel, additional experimental data are required that would allow one to determine (at least qualitatively) the profile of the current transported by superthermal and runaway electrons generated by the RF wave. The measurements of the chord intensity profiles of SXR bremsstrahlung can provide such additional data. In these experiments, the SXR profiles were measured with a seven-channel X-ray spectrometer behind different filters, which allowed us to determine the distribution of the SXR intensity along the major radius of the plasma column in one discharge. A set of filters (Be foils with thickness from 100 to 600 μm and 1-mm Al and 1-mm Pb filters) and a set of relatively calibrated photomultipliers and thin (3 mm) polystyrene scintillators allowed us to analyze SXR emission in the energy range of 2 keV $\le E_{h\nu} \le$ 30 keV. Figure 14 shows the intensity profiles of SXR emission with different hardnesses measured in the OH mode (25 ms) and during the first several milliseconds of the RF pulse (27.9 ms) in shot series no. 051216. The figure compares the SXR intensities in the different spectral ranges measured behind three filters (100-μm Be, 400-μm Be, and 1-mm Pb + 100-μm Be foils): (i) $E_{h\nu} > 2$ keV, (ii) $E_{h\nu} > 4$ keV and (iii) 20 keV $< E_{h\nu} <$ 30 keV. It is seen that the second maximum in the SXR profile forms at $r = 2$–6 cm during LHCD (27.9 ms). This maximum is produced by substantially harder photons than those forming the central peak. We suppose that the sources of this radiation are superthermal and runaway electrons generated by the RF wave and localized just at $r = 2$–6 cm. Their location correlates with the shape of the J_{RF} profile shown in Fig. 9a.

6. CONCLUSIONS

In the LHCD experiments carried out with deuterium plasma at the FT-2 tokamak, electron heating

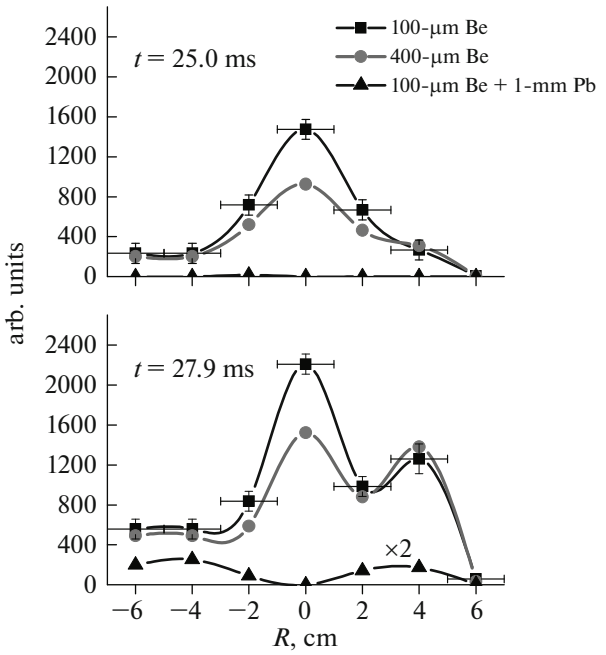

Fig. 14. Profiles of the SXR intensity measured with a seven-channel X-ray spectrometer behind different filters in the OH (25 ms) and LHCD (27.9 ms) regimes in different spectral ranges: $E_{h\nu} > 2$ keV (100-μm Be), $E_{h\nu} > 4$ keV (400-μm Be), and 20 keV $< E_{h\nu} <$ 30 keV (100-μm Be + 1-mm Pb). The maximum measured photon energy $E_{h\nu}$ is determined by the ability of a 3-mm-thick polystyrene scintillator to respond only to SXR photons with energies of $E_{h\nu} < 30$ keV.

was observed in the central region of the plasma column. At the initial plasma density of $\langle n_e \rangle = (1.6–1.9) \times 10^{19}$ m^{-3}, the central electron temperature increased from 550 to 750 eV. Central electron heating was accompanied by an increase in the plasma density and cooling of the edge plasma. The observed effect cannot be caused by thermalization of superthermal electrons, because the time of their collisional thermalization is much longer than the RF pulse, $t_E \approx 100–200$ ms $\gg \Delta t_{RF}$. Central electron heating, as well as the increase in the plasma density, can be explained by a transition into the ICC mode. According to the experimental data, the threshold power for this effect is $\Delta P_{RF}^{th} = P_{input} - P_{output} \geq 63$ kW. Complex simulations carried out using a special software package have shown that the mechanism for the transition into the improved confinement mode at $r < 3$ cm can be associated with the suppression of electron heat transport due to the broadening of the plasma current channel in the course of lower hybrid drive of the current carried by superthermal and runaway electrons. In this case, according to the Bohm and gyro-Bohm models [2, 7], the decrease in the magnetic shear to $s = (r/q)(dq/dr) \leq 0$ should result in a substantial decrease in both thermal diffusivity χ_{eff} and diffusion coefficient D_{eff} [3]. While heat transport in the plasma core is suppressed, the residual ohmic power remains sufficient to additionally heat electrons in the central region of the plasma column. At the same time, the decrease in the OH power results in electron cooling at the plasma edge. To experimentally confirm the hypothesis on broadening of the profile of the current density $J_{sum}(r, t) = J_{RF}(r, t) + J_{OH}(r, t)$ during LHCD, the chord profiles of the SXR bremsstrahlung intensity were measured. The results of these measurements indicate that the current density profile $J_{RF}(r, t)$ forms at radii of $r = 2–6$ cm, which correlates with the localization of the J_{RF} profile used in numerical simulations (see Fig. 9a). Unfortunately, we failed to directly measure the change in the profile of the plasma current channel. However, analysis of the experimental data and complex simulations performed on their basis allow us to assume that the observed effect of central heating is associated with the transition into the ICC mode, moreover, taking into account that it is a threshold effect. The issues related to the change in the profile of the current channel and the observed change in the heat transport in the plasma column during LHCD will be subjects of our further research.

ACKNOWLEDGMENTS

This work was supported in part by the Russian Science Foundation, grant no. 17-12-01110.

REFERENCES

1. Y. Baranov, V. Basiuk, G. Calabro, A. Cardinali, C. Castaldo, R. Cesario, J. Decker, D. Dodt, A. Ekedahl, L. Figini, J. Garcia, G. Giruzzi, J. Hillairet, G. T. Hoang, A. Hubbard, et al., Plasma Phys. Controlled Fusion **52**, 124031 (2010).
2. X. Litaudon, Y. Peysson, T. Aniel, G. Huysmans, F. Imbeaux, E. Joffrin, J. Lasalle, P. Lotte, B. Schunke, J. L. Segui, G. Tresset, and M. Zabiego, Plasma Phys. Controlled Fusion **43**, 677 (2001).
3. T. J. J. Tala, J. A. Heikkinen, V. V. Parail, Y. F. Baranov, and S. J. Karttunen, Plasma Phys. Controlled Fusion **43**, 507 (2001).
4. S. I. Lashkul, A. B. Altukhov, A. D. Gurchenko, V. V. D'yachenko, L. A. Esipov, M. Yu. Kantor, D. V. Kuprienko, M. A. Irzak, A. N. Saveliev, A. V. Sidorov, A. Yu. Stepanov, and S. V. Shatalin, Plasma Phys. Rep. **36**, 751 (2010).
5. S. I. Lashkul, A. B. Altukhov, A. D. Gurchenko, E. Z. Gusakov, V. V. D'yachenko, L. A. Esipov, M. A. Irzak, M. Yu. Kantor, D. V. Kuprienko, A. N. Saveliev, A. Yu. Stepanov, and S. V. Shatalin, Plasma Phys. Rep. **41**, 990 (2015).
6. A. E. Shevelev, E. M. Khilkevitch, S. I. Lashkul, V. V. Rozhdestvensky, A. B. Altukhov, I. N. Chugunov, D. N. Doinikov, L. A. Esipov, D. B. Gin, M. V. Iliasova, V. O. Naidenov, N. S. Nersesyan, I. A. Polunovsky, A. V. Sidorov, and V. G. Kiptily, Nucl. Instrum. Meth. Phys. Res. A **830**, 102 (2016).

7. Y. Peysson and the TORE SUPRA Team, Plasma Phys. Controlled Fusion **42**, B87 (2000).
8. V. Pericoli Ridolfini, G. Calabro, L. Panaccione, FTU team, and ECH team, Nucl. Fusion **45**, 1386 (2005).
9. S. V. Mirnov, *Physical Processes in Tokamak Plasmas* (Energoatomizdat, Moscow, 1985) [in Russian].
10. S. I. Lashkul, A. B. Altukhov, V. V. D'yachenko, L. A. Esipov, M. Yu. Kantor, D. V. Kuprienko, A. D. Lebedev, Ya. A. Nikerman, and A. Yu. Popov, Plasma Phys. Rep. **38**, 851 (2012).
11. S. I. Lashkul, A. B. Altukhov, A. D. Gurchenko, E. Z. Gusakov, V. V. Dyachenko, L. A. Esipov, M. Yu. Kantor and D. V. Kouprienko, in *Proceedings of the 42nd EPS Conference on Plasma Physics, Lisbon, 2015,* ECA **39E**, P5.173 (2015).
12. M. A. Irzak and O. N. Shcherbinin, Nucl. Fusion **35**, 1341 (1995).
13. D. Piliya and A. N. Saveliev, Preprint JET_R(98) 01 (JET Joint Undertaking, Abingdon, 1998).
14. F. Romanelli and F. Zonca, Phys. Fluids B **5**, 4081 (1993).

Translated by I. Grishina